

Supplement of Atmos. Chem. Phys., 14, 13023–13041, 2014
<http://www.atmos-chem-phys.net/14/13023/2014/>
doi:10.5194/acp-14-13023-2014-supplement
© Author(s) 2014. CC Attribution 3.0 License.



Supplement of

An improved dust emission model – Part 1: Model description and comparison against measurements

J. F. Kok et al.

Correspondence to: J. F. Kok (jfkok@ucla.edu)

Supplementary Methods

This supplementary document contains detailed descriptions of the analysis of each data set in the quality-controlled compilation of vertical dust flux data sets. The resulting values of u_{*t} , α and C_d for each data set are summarized in Table S1, and plotted in Fig. 4 of the main article. For each data set we also show the measured dust flux F_d as a function of u_* in Figs. S2 and S3, along with our parameterization of the vertical dust flux (Eq. 18), and the parameterizations of Gillette and Passi (1988) and Marticorena and Bergametti (1995).

1 The Gillies and Berkofsky (2004) data sets (GB04)

This study was performed in the spring of 2000 at Owens Lake in California, which is a mostly dry lake at an elevation of 1084 m that constitutes a major source of dust emissions in the U.S. (Gillette et al., 1997). Measurements were performed at two locations; the northern site was designated as the northern sand sheet (NSS), for which the soil was characterized by loose coarse sand moving over a discontinuous soil crust. The southern site was west of the town of Keeler (KS), for which the soil was similar to NSS, although more heavily crusted. Both sites were flat, devoid of vegetation and other non-erodible roughness elements, and had upwind fetch (i.e., uninterrupted upwind area generating dust emissions) in excess of 5 km.

1.1 Description of measurements

Gillies and Berkofsky (2004) used fast-response aerosol monitors (TSI Model 8520 DustTrak) to measure mass concentration of particulate matter $\leq 10 \mu\text{m}$ aerodynamic diameter (PM10) at three or four logarithmically-spaced heights between 1.7 and 9 meters. Simultaneously, wind speed was measured at 5 heights. The saltation activity at the sites was also monitored with a Sensit instrument (Stockton and Gillette, 1990), mounted at a height of around 15 cm. However, these data were deemed unreliable (Gillies, personal communication, 2012), and were therefore not used in our analysis.

1.2 Analysis of data sets

We analyzed the original measurements of wind speed and dust concentration, each averaged over time intervals of 1 minute. These measured data include 4 dust emission events at KS, and 1 at NSS. The data from this latter event was too sparse to determine the soil threshold friction velocity, and was therefore not used. Of the 4 events at KS, we used the 2 events for which there was sufficient data to determine the threshold u_{*t} . These events occurred on February 16, 2000 from 11:12 - 15:03 hours, and on March 20, 2000 from 7:00– 9:50 hours. The range of u_* measured during these events was 0.26 – 0.43 m/s and 0.33 – 0.62 m/s, respectively.

Gillies and Berkofsky (2004) did not report the soil texture at their measurement sites. However, extensive soil surveys in the area were commissioned by the Great Basin Unified Air Pollution Control District, and performed by Soil and Water West Inc. (2001). In particular, 4 soil surveys that measured the soil texture at a 1 or 2 cm depth onwards were made within an estimated 1 km from the KS site. We use the average of these 4 determinations, resulting in a clay fraction of $9.1 \pm 2.0 \%$, silt fraction of $9.1 \pm 3.0 \%$, sand fraction of $81.8 \pm 5.0 \%$, and thus a soil texture of loamy sand.

The 1-minute resolution data sets of wind speed and dust concentration were analyzed using a running average over 30 minutes (see Section 3.2 in the main text). The soil friction velocity was then calculated from the best fit with the logarithmic law of the wall (Prandtl, 1935), and the

vertical dust flux was obtained from the vertical profile of the dust concentration, as described in Appendix C.

We corrected the measured aerodynamic PM10 vertical dust flux to the desired $\leq 10 \mu\text{m}$ geometric diameter flux by multiplying by 1.42 ± 0.10 (see Section 3.2 in the main text). Furthermore, a correction needed to be made to account for the sub-isokinetic sampling conditions caused by the use of a nozzle intake velocity that was less than the ambient wind speed (Gillies and Berkofsky, 2004). Based on manufacturer laboratory tests, the collection efficiency of the used DustTrak samplers was between 60 and 95 % (Houser and Nickling, 2001; Gillies and Berkofsky, 2004). We therefore corrected the GB04 vertical dust flux data by multiplying by a factor of $(0.60 \times 0.95)^{-1/2} = 1.32 \pm 0.30$.

The soil threshold friction velocities for the February 16 and March 20 data sets were estimated using the Taylor series method detailed in Appendix B (see Figs. S4a and S4b), yielding 0.24 ± 0.020 and 0.31 ± 0.02 m/s for the February 16 and March 20 events, respectively. Using these estimated thresholds, the fragmentation exponent α and dust emission coefficient C_d were calculated by fitting the dimensionless dust flux as a function of dimensionless friction velocity to Eq. (21) (see Table S1 and Figs. S4a and S4b).

2 The Zobeck and Van Pelt (2006) data sets (ZP06)

This study was performed in March 2003 on an experimental plot of the U. S. Department of Agriculture Agricultural Research Service in Big Spring, Texas, at an elevation of 744 m. The authors chiseled bare a flat round study field of 100 m in radius, and erected ridges around the field to prevent the escape or influx of saltators. Fields upwind and downwind were not erodible. The soil of the study field was an Amarillo fine sandy loam (13% clay, 9% silt, and 78% sand).

2.1 Description of measurements

The authors erected three measurement towers on the field, which were aligned along the dominant wind direction, and were placed 100 m apart at the upwind (~western), center, and downwind (~eastern) edge of the field (see Fig. 1 in Zobeck and Van Pelt (2006)). The western tower was present only in the first set of measurements on March 4th, after which it was moved to a location downwind of the field. The uninterrupted fetch was thus ~200 m for the eastern tower.

At each of the towers, the authors measured the aerodynamic PM10 aerosol concentration using DustTrak aerosol samplers at 2, 5, and 10 m height. These aerosol samplers were fitted with a customized orifice to provide isokinetic sampling in typical dust-emitting winds (see Fig. 3 in Zobeck and Van Pelt (2006)). The tower in the center of the field was also fitted with cup anemometers at heights of 0.5 and 2 m to measure wind speed. Finally, a Sensit piezoelectric particle impact detector (Stockton and Gillette, 1990) was used at the central tower to measure the impact flux of saltators at the soil surface.

2.2 Analysis of data sets

We analyzed the original measurements of wind speed, dust concentration, and Sensit measurements, each of which was averaged over a 1 minute interval. These data comprised the 3 dust storm events on March 4, 18, and 27 of 2003 reported in Zobeck and Van Pelt (2006). We were unable to use the data from the last event because the maximum 30-minute average friction velocity barely exceeded threshold conditions, such that reliably determining the fragmentation exponent α and dust emission coefficient C_d from these data was not possible. For the other two

events, we used data for time periods during which saltation was occurring consistently. This corresponds to 12:02 – 16:04 hours for the March 4th event and to 10:23 – 12:49 hours for the March 18th event. The range of u_* measured during these events was 0.39 – 0.54 m/s and 0.38 – 0.48 m/s, respectively.

We calculated the friction velocity by fitting the logarithmic law of the wall (Eq. C.3) to the wind speed measured at heights 0.5 and 2 m.

2.2.1 Correction for limited fetch

The vertical dust flux can be calculated from the dust concentrations at the 3 measurement heights using the method of Appendix C. However, as mentioned above, the fetch of the field was only 200 m, which was on the order of the flux footprint (i.e., the upwind area that contributes substantially to the concentration at the measurement location) (Schuepp et al., 1990). Therefore, the measured concentrations should be corrected for the effect of the limited fetch before the vertical dust flux can be calculated.

Fortunately, the experimental design of Zobeck and Van Pelt (2006) is highly conducive to such a correction because this study measured the background PM10 concentration of air unaffected by the emission of dust from the experimental field. We therefore obtain the concentration of PM10 dust originating from emission from the 200 m diameter erodible field by subtracting this background PM10 concentration. For the measurements on March 4th, the background concentration was estimated from the upwind PM10 measurements at the western edge of the field (see Fig. 1 in Zobeck and Van Pelt (2006)). That is, a 1-minute temporal resolution record of the PM10 background concentration was obtained by averaging the measurements at the 3 heights, which were within 30 %. We then calculated the 30-minute running mean of the PM10 background concentration, which was then subtracted from the measurements at the eastern tower. For the measurements on March 18th, no measurements were made at the upwind boundary of the field. To nonetheless estimate the PM10 background concentration, we used the measurements at 10 m height at the center tower. Furthermore, in order to make sure that we only analyzed measurements due to dust emission and not due to fluctuations in measurements of the background PM10, we discarded measurements that did not exceed the background PM10 by two standard deviations of the 30 1-minute measurements comprising the 30-minute running mean of the background PM10 concentration.

After extracting the portion of the PM10 concentration due to local dust emission in the manner described above, we applied a correction for the limited fetch using the parameterization of Kormann and Meixner (2001). That study used boundary layer theory to derive an expression for the concentration c at height z produced by a line source q at ground level, at an upwind distance x from the measurement location. That is,

$$c(x, z) = \frac{qr\xi^\mu}{\Gamma(\mu)C_u z^{1+m} x^\mu} \exp(-\xi/x), \quad (\text{S.1})$$

where Γ is the gamma function, and the constant C_u and the exponent m are defined by fitting the wind profile in the vicinity of z by a power law:

$$U(z) = C_u z^m. \quad (\text{S.2})$$

Since the mean wind speed U follows the logarithmic profile of Eq. (A.3), this yields

$$m = \frac{1}{\ln(z/z_0)}, \quad (\text{S.3})$$

such that for typical values of z (1 – 10 m) and z_0 (10^{-5} – 10^{-2} m), we have that $m \approx 0.1 - 0.2$ (e.g., Fig. 2 in Kormann and Meixner, 2001). We further have that

$$\mu = (1 + m) / r, \quad (\text{S.4})$$

$$r = 2 + m - n, \text{ and} \quad (\text{S.5})$$

$$\xi(z) = \frac{C_U z^r}{r^2 \kappa}. \quad (\text{S.6})$$

Finally, the eddy diffusivity power law exponent n lies between 1 and 1.5 for neutral or unstable conditions typical of dust emission events. Specifically,

$$n = \frac{1 - 24z / L}{1 - 16z / L}, \quad (\text{S.7})$$

where L is the Obukhov length, which scales the height at which mechanical production of turbulence through wind shear equals the buoyant production of turbulence (Kaimal and Finnigan, 1994). We take $L = -25$ m, which is typical for daytime conditions over land (see p. 25 in Kaimal and Finnigan (1994)); note that a different choice of L that is characteristic of daytime conditions, between approximately -10 and -200 m, has a negligible impact on our results.

The concentration due to an upwind area with extend x_L is then

$$C(x_L, z) = \int_0^{x_L} c(x, z) dx = Q \int_0^{x_L} \frac{r \xi^\mu}{\Gamma(\mu) C_U z^{1+m} x^\mu} \exp(-\xi / x) dx. \quad (\text{S.8})$$

The correction factor to convert the measured concentration to the concentration that would have been measured had the fetch been unlimited is thus

$$f_c(x_L, z) = \frac{\int_0^{\infty} \frac{r \xi^\mu}{\Gamma(\mu) C_U z^{1+m} x^\mu} \exp(-\xi / x) dx}{\int_0^{x_L} \frac{r \xi^\mu}{\Gamma(\mu) C_U z^{1+m} x^\mu} \exp(-\xi / x) dx}, \quad (\text{S.9})$$

where the fetch $x_L = 200$ m.

2.2.2 Obtaining u^*_t , α , and C_d

We corrected the measured concentration by first subtracting the background PM10 in order to extract the fraction of the measured concentration due to local erosion upwind of the sensor, rather than from advection. We then corrected the measured aerodynamic PM10 concentration to the desired geometric ≤ 10 μm geometric diameter mass concentration by multiplying by 1.42 ± 0.10 (see Section 3.2 in the main text). Finally, we multiplied the obtained dust concentration by the correction factor of Eq. (19) in order to obtain the geometric 0 – 10 μm diameter mass concentration at a given measurement height that would have been produced by an erodible field with unlimited upwind fetch. Finally, we compute the vertical dust flux from the concentration measurements corrected in the above manners by using Eq. (C.5) for the measurements at 2 and 5 m for the eastern tower. (Note that we did not use the measurements at 10 m height because these measurements in many cases were not elevated above the background PM10 concentration despite the occurrence of saltation, indicating that the dust plume did not regularly reach this measurement height.) We estimate the relative uncertainty on the vertical dust flux due to fetch correction to be

50%, which, like the uncertainty arising from the correction from aerodynamic to geometric concentration, is propagated into the uncertainty on the value of C_d extracted from the ZP06 data sets (see Appendix A).

The soil threshold friction velocity for both the March 4 and March 18 data sets were estimated using the Taylor expansion method (see Figs. S4c and S4d, and Appendix B), yielding $u_{*t} = 0.41 \pm 0.03$ m/s and 0.36 ± 0.03 m/s, respectively. Note that the threshold for March 4th was somewhat difficult to determine because of significant scatter in F_d for u^* close to u_{*t} (Fig. S4c). To further investigate whether the u_{*t} values obtained from the Taylor expansion method were realistic, we also calculated the threshold u^* with the Time Fraction Equivalence Method (Stout and Zobeck, 1997), using the 1-minute resolution Sensit measurements of the saltation impact flux. This yielded threshold u^* values of 0.39 and 0.33 m/s for the March 4th and 18th events, respectively, thereby supporting the values of u_{*t} obtained using the Taylor expansion method.

Using the estimated values of u_{*t} , the fragmentation exponent α and dust emission coefficient C_d were estimated by fitting the dimensionless dust flux as a function of dimensionless friction velocity to Eq. (21) (see Table S1 and Figs. S5c and S5d). A second estimate of α was obtained by fitting Eq. (24) to the measured ratio of the vertical dust and horizontal saltation flux (Figs. S6a and S6b).

3 The Fratini et al. (2007) data sets (FC07)

Fratini et al. (2007) used eddy covariance to measure the flux of dust emitted in May 2005 by eroding soils in the Ejin'a area of the Alashan Prefecture, located in the Gobi desert in Inner Mongolia, China. Their site, denoted as GB1 and located at 960 m above sea level, consisted of bare soil (termed *internebkhas*) sparsely interspersed with shrubs that were partially covered by small, sandy dunes (termed *nebkhas*). Approximately 25% of the soil surface of the internebkhas was covered with pebbles, with the remaining 75% composed of erodible particles, with a median diameter of ~ 225 μm (see Table 3 in Fratini et al. (2009)).

The soil texture of both the nebkhas (0.1 % clay, 7.1 % silt, and 92.8 % sand) and the internebkhas (0.8 % clay, 10.4 % silt, and 88.9 % sand) was sand. The fetch length at the measurement site was in excess of 5 km.

3.1 Description of measurements

Fratini et al. (2007) used a high frequency 3D ultrasonic anemometer, located at 12 m height from the surface, to determine the friction velocity directly from the turbulence parameters. The dust particle concentration was measured using an optical particle counter (OPC), which measured particles with aerodynamic diameters between 0.35 and 9.5 μm . These measurements were thus corrected to the geometric size range using equation (19) in the main text and equation (6) in Kok (2011b), resulting in a multiplication by 1.52 ± 0.12 . However, the efficiency of the air inlet system was not tested and could have produced an under-sampling of larger particles and thus an underestimation of the total dust flux (Fratini, personal communication, 2012). This is also suggested by the relatively low contribution of aerosols with diameter larger than 5 μm , in comparison to other size-resolved measurements of the vertical dust flux (Gillette et al., 1972; Gillette, 1974; Gillette et al., 1974; Sow et al., 2009; Shao et al., 2011).

Fratini et al. (2007) used eddy co-variance to calculate the vertical dust flux from the measured particle concentration and 3D wind speed. In addition, Fratini et al. (2009) modeled the volumetric soil water content from measurements of temperature, ambient relative humidity, and soil texture. The average soil volumetric water content was derived as a weighted average of

water content in the *nebkhas* (the small dunes) and the *internekhkas* (bare soil), according to the fraction of each type of soil at GB1. The resulting volumetric soil water content ranged between 1% and 2% for the May 25 dust event analyzed in Fratini et al. (2007), which could have somewhat elevated the threshold for dust emission since the soil's clay content was very low (Fecan et al., 1999). Note that Fratini et al. (2007, 2009) did not measure the saltation flux.

We analyzed the original data sets of wind direction, friction velocity, and vertical dust flux, all of which had temporal resolutions of 10 minutes.

3.2 Analysis of data sets

Wind erosion at the GB1 site occurred predominantly when the wind blew from the direction that allowed it to mobilize the sand in the *nebkhas*, which then proceeded to emit dust through sandblasting the *internebkhas* soil (Fratini et al., 2009). This wind direction corresponded to northeasterly winds; since wind erosion observed for other wind directions was thought to be supply-limited (Fratini et al., 2009), we did not use these data. Specifically, we only used the data from the main dust event on May 25th, during which the wind direction ranged between 60° and 110°. Winds from this direction produced a substantial vertical dust flux (see Fig. 8 in Fratini et al. (2009)). Since there is a gap in data collection from 10:20 until 12:00 local time due to insufficient data quality (Fratini, personal communication, 2012), we split the May 25th data into two cases, with Event 1 containing the data from 0:40 – 10:20 hours, and Event 2 containing the data from 12:00 – 23:50 hours.

For both Event 1 and Event 2, u_{*t} is difficult to determine using the Taylor expansion method due to scarce and scattered data near the threshold. For Event 1, we therefore take the soil threshold friction velocity in between the 3 data points at the lowest u^* (0.236 ± 0.005 m/s) and the minimum u^* for wind erosion at the elevation at which measurements were taken (0.170 m/s), for a u_{*t} of 0.203 ± 0.016 m/s. The range of u^* during Event 1 was $0.232 - 0.693$ m/s. For Event 2, several measurements show positive vertical dust fluxes for friction velocities very close to 0.17 m/s, which is the minimum u_{*t} for wind erosion at the measurement elevation (see Eq. 6). We therefore take $u_{*t} = 0.170 \pm 0.014$ m/s. The range of u^* during Event 2 was $0.171 - 0.606$ m/s. This slightly lower u_{*t} for Event 2 relative to Event 1 is consistent with the drying out of the soil during the course of the day, as predicted by the soil moisture model in Fratini et al. (2009) (Fratini et al., 2009). Moreover, the relatively low values of u_{*t} for both cases are consistent with the low soil moisture during these events (Fratini et al., 2009), and the high susceptibility to erosion of the sandy deposits of the *nebkhas* that then proceed to sandblast the *internebkhas*.

Using the estimated values of u_{*t} , the fragmentation exponent α was estimated through fitting of the dimensionless dust flux as a function of dimensionless friction velocity to Eq. (21) (see Table S1 and Figs. S5e and S5f). Note that we could not obtain estimates of the dust emission coefficient C_d from the Fratini et al. data sets because the measurement locations were not homogeneous due to the presence of the *nebkhas* (see main text). Moreover, ~25% of the surface of *internebkhas* were covered by non-erodible pebbles (Fratini et al., 2009), shielding the soil from saltation impacts in a poorly understood manner.

4 The Sow et al. (2009) data sets (SA09)

Sow and colleagues (Sow, 2009; Sow et al., 2009) performed measurements of the size-resolved vertical dust flux as part of the African Monsoon Multidisciplinary Analysis (AMMA) study in the summers of 2006 and 2007. Their experimental site was near the AMMA supersite

of Banizoumbou, which is located about 60 km east of Niamey, the capital of Niger. Specifically, their measurements were performed in the middle of an agricultural field, with a fetch varying between 190 and 575 m, depending on wind direction (see Fig. 2 in Rajot et al., 2008). The site is located 250 m above sea level (Rajot et al., 2008).

Measurements of the soil texture were not reported in Sow et al. (Sow, 2009; Sow et al., 2009). However, Rajot et al. (2003) reported the soil texture for a field within several km of the Sow et al. (Sow et al., 2009) measurement site as sandy, with 2.8% clay, 2.4% silt, and 94.8% sand. This is also consistent with the soil texture for this region in the Food and Agriculture Organization (FAO) soil database (FAO, 2012), which lists the dominant soil texture in the area containing the Sow et al. (2009) experimental site as sand, with 5% clay, 5% silt, and 90% sand.

Since measurements were made on an agricultural field, the soil contained residue of crop cover, which absorbed momentum from the wind and reduced the shear stress on the soil for a given value of u'_* .

4.1 Description of measurements

Sow et al. used both optical particle counters and Tapering Element Oscillating Microbalances (TEOMs) to measure the concentration of dust at the heights of 2.1 and 6.5 m. They simultaneously measured the wind speed at heights of 0.35, 0.8, 1.5, 2.32, and 4.75 m, which they used to obtain the wind friction velocity and aerodynamic roughness length z_0 (defined by Eq. C.3 in Appendix C). The vertical dust flux was calculated using the gradient method (see Appendix C). Sow et al. (2009) also measured the saltation impact flux using a Saltiphone instrument (Spaan and van den Abeele, 1991) in 2006, and a Sensit instrument (Stockton and Gillette, 1990) in 2007, both mounted at ~ 7 cm height above the surface.

Sow et al. (2009) reported measurements made during three dust storm events, two of which were due to monsoon flow (termed ME1 and ME4), and one was due to a convective event (termed CE4).

4.2 Analysis of data sets

We analyzed measurements of the events ME1 and CE4, and were unable to use the measurements of the ME4 event because its duration of 39 minutes (table 1 in Sow et al., 2009) was on the order of the averaging time of 30 minutes. We used the measurements of ME1 from 01:46 – 03:43 hours on June 23 2006. The event CE4 started at 21:37 hours on June 22, 2007, and lasted until 00:11 hours on June 23 2007. Unfortunately, one of the two TEOMs ceased functioning after 23:30 hours, such that vertical dust flux measurements are unavailable after that time. Saltation flux measurements were available during the entire storm period.

We determined the mean fetch for both events by obtaining the wind direction during the events from Figure 32 in Sow (2009), and calculating the fetch for each wind direction from the aerial photograph of the measurement site provided in Rajot et al. (2008). This procedure yielded a fetch of 575 m for ME1, and 420 m for CE4. According to the parameterization of Kormann and Meixner (2001), which is discussed in Section 2.2, the fraction of the measured concentration due to local erosion upwind of the sensor, rather than from advection, would have been substantially higher than measured if the fetch had been infinite. Consequently, it would be desirable to make a correction for the limited fetch. Unfortunately, this is not possible in the case of the Sow et al. (2009) measurements because, unlike for the Zobeck and Van Pelt (2006) measurements, no measurements of the background concentration are available (see Fig. 28 in Sow, 2009). Moreover, because of the advection of dust from local and regional dust sources,

this ‘background’ concentration was likely to be highly variable in time. However, despite the problem of the limited fetch, the Sow et al. (2009) data set is well-behaved, with a clearly defined threshold u_* (Figs. S4e and S4f), and relatively little scatter in the measured dust flux (Fig. S5g and S5h). The variation of the measured dust flux with u_* thus seems realistic, such that we neglect the limited fetch and use the Sow et al. (2009) data sets in our analysis.

We analyzed the original measurements of wind friction velocity and saltation impact flux measurements for the ME1 event, both as 15-minute running means with 1-minute resolution. For CE4, we obtained the 15-minute running mean of wind friction velocity, and the 1-minute resolution saltation impact flux measurements from Figure 7 in Sow et al. (2009). For both ME1 and CE4, we obtained the TEOM measurements from Figure 28 in Sow (2009). Since the resolution of these measurements was 2 minutes, we interpolated these to 1-minute resolution in order to match the temporal resolution of the wind friction velocity and saltation impact flux measurements. Further, the maximum aerodynamic size of dust particles measured by the TEOM, which is determined by the aerodynamic properties of a specially-designed inlet (see Fig. 3 in Rajot et al., 2008), was $\sim 40 \mu\text{m}$, corresponding to $D_d \approx 30 \mu\text{m}$ per Eq. (19). Part of this size range is outside of the validity of the theoretical size distribution of Kok (2011b), which covers the size range $0 - 20 \mu\text{m}$. To convert the measured size range to the geometric $10 \mu\text{m}$ range we therefore assume that the contribution of the size range of $20 - 30 \mu\text{m}$ is half that of the $0 - 20 \mu\text{m}$ size range. We estimate the relative error in this conversion from $\leq 30 \mu\text{m}$ to $\leq 10 \mu\text{m}$ geometric diameter flux at $\pm 30 \%$, which is propagated into the uncertainty on the value of C_d extracted from the Sow et al. measurements (see Appendix A).

As mentioned above, the Sow et al. (2009) experimental site contained roughness elements, mainly in the form of crop residue. These roughness elements absorb wind momentum, such that their presence needs to be corrected for in order to determine u_* and u_{*t} . We discuss the procedure for making this correction below.

4.2.1 Correction for roughness elements

In order to correct for the presence of roughness elements at the Sow et al. (2009) experimental site, we use the semi-empirical formula of Marticorena and Bergametti (1995). This formula relates the ratio of the wind friction velocity (u'_*) and the bare soil friction velocity (u_*) to the ratio of the soil’s aerodynamic roughness length in the presence (z_0) and in the absence (z_{0s}) of the roughness elements. Specifically,

$$f_{\text{eff}} \equiv \frac{u_*}{u'_*} = 1 - \frac{\ln\left(\frac{z_0}{z_{0s}}\right)}{\ln\left[0.70\left(\frac{10}{z_{0s}}\right)^{0.8}\right]}, \quad (\text{S.10})$$

where $z_0 \approx D_{\text{med}}/15$ for a mixed soil (Greeley and Iversen, 1985; Sherman, 1992), and where $D_{\text{med}} = 274 \mu\text{m}$ is the soil’s median particle size from the soil size distribution provided in Table IV.4 of Sow (2009). Note that Eq. (S.10) includes a correction to a small error in Eq. (20) of Marticorena and Bergametti (1995) described in King et al. (2005).

We use the soil aerodynamic roughness lengths measured by Sow et al. (2009), which were 1.7 mm and 3.7 mm for events ME1 and CE4, respectively (see Table 1 in Sow et al. (2009) and Fig. 32 in Sow (2009)). These roughness lengths were measured during the storms events, and thus include a small contribution of the roughness generated by saltating particles (Owen, 1964).

However, this contribution was negligible compared to the aerodynamic roughness of the field (Alfaro, personal communication, 2012). Using these values of z_0 yields values of f_{eff} of 0.56 ± 0.06 and 0.48 ± 0.05 , where we estimated the relative uncertainty on f_{eff} at $\sim 10\%$ from Figure 4 in King et al. (2005), which compares measured values of f_{eff} against values computed with Eq. (S.10). Note that f_{eff} , and its uncertainty, does not affect the determination of α and C_d , since these are determined through a regression of F_d against u^*/u_{*t} (see Eq. 21), which is unaffected by f_{eff} .

4.2.2 Obtaining u_{*t} , α , and C_d

The u^* values calculated with the above procedure during the storm events ranged from 0.238 to 0.321 m/s for ME1 and from 0.314 to 0.358 m/s for CE4. We estimated the soil threshold friction velocity for the ME1 and CE4 data sets from the saltation impact flux measurements using the Taylor expansion method (see Figs. S4e and S4f, and Appendix B), resulting in u_{*t} values of 0.237 ± 0.019 m/s for ME1 and 0.232 ± 0.019 m/s for CE4.

Using these estimated thresholds, the fragmentation exponent α and dust emission coefficient C_d were estimated through fitting of the F_d as a function of u^*/u_{*t} to Eq. (21) (see Figs. S6g and S6h). A second estimate of α was made by fitting Eq. (24) to the measured ratio of the vertical dust and horizontal saltation impact fluxes (see Figs. S6c and S6d).

5 The Shao et al. (2011) data set (SI11)

The recent study of Shao et al. (2011) reported measurements of the vertical dust flux generated by a strong erosion event during the Japanese Australian Dust Experiment (JADE). This field campaign took place from February 23 to March 13, 2006 on a flat, fallow agricultural field in southeastern Australia, near the town of Mildura, Victoria. The elevation at the site was 97 m, and the fetch length of the field was ~ 800 m in the western direction, ~ 200 m in the eastern direction, and in excess of 1 km in the north and south directions (Ishizuka et al., 2008).

The soil texture was loamy sand, with 11% clay, 35% silt, and 54% sand (Shao et al., 2011). The soil surface consisted of 84% bare soil, 2% crusts, 12% mobile litter (wheat plant residuals), and 2% non-erodible elements in the form of rocks and tree litter.

5.1 Description of measurements

Ishizuka et al. (2008, 2014) and Shao et al. (2011) used optical particle counters at 1.0, 2.0, and 3.5 m heights to measure the particle concentration in the 0.3–8.4 μm geometric diameter size range (Ishizuka, 2012, personal communication). Simultaneous wind speed measurements were made with anemometers at 0.5 and 2.16 m height. These measurements were combined to calculate the vertical dust flux as a function of friction velocity using the gradient method (see Appendix C), with an added correction for the gravitational settling of dust particles, which causes the dust flux to not be entirely constant with height, as assumed by the gradient method (see Shao et al. (2011), p. 10).

Ishizuka et al. (Ishizuka et al., 2008) and Shao et al. (2011) also reported the saltation flux at heights of 0.05, 0.1, 0.2, and 0.3 m using Sand Particle Counters (Yamada et al., 2002). In addition, the volumetric soil moisture content of the topsoil was measured using time domain reflectometry soil moisture sensors.

5.2 Analysis of data sets

We analyzed the original data sets of friction velocity, vertical dust flux, soil moisture, and saltation flux at 5 cm height for the strong erosion event that occurred on March 12, 2006 and was analyzed by Shao et al. (2011). The measurements in these data sets were averaged over 1 minute.

We used data from the time period during which the dust flux was positive and saltation was approximately continuous, corresponding to 10:25 – 17:46 hours (Ishizuka et al., 2008; Ishizuka et al., 2014). During this time, the wind blew from the NW – N direction, such that the fetch was in excess of 1 km and substantially larger than the flux footprint (Schuepp et al., 1990). The range of u^* during the event, with the correction for roughness elements discussed below, was 0.164 – 0.246 m/s.

We corrected the measured flux in the 0.3 – 8.4 μm geometric diameter range to the desired 0 – 10 μm size range through multiplication by 1.22, following Eq. (6) in Kok (2011b). Moreover, we convert the measured particle concentration to dust mass flux assuming a dust particle density of 2500 kg/m³, consistent with the density of both natural dust aerosols (Kaaden et al., 2009) and the density of the Arizona test dust with which the DustTrak aerosol monitors used by the GB04 and ZP06 data sets were calibrated (Wang et al., 2009; TSI Inc., 2012).

The volumetric moisture content in the topsoil during the event was $2.35 \pm 0.19 \%$, and thus very close to the threshold ($\sim 2 \%$ for a soil with 11 % clay content) at which soil moisture starts increasing u_{*t} (Fecan et al., 1999). The effect of the soil moisture on u_{*t} was thus likely small, consistent with the low value of u_{*t} determined by our analysis (see below).

5.2.1 Correction for roughness elements

As was the case for the data set of Sow et al. (2009), the experimental site of Shao et al. (2011) contained non-erodible roughness elements, the effect of which needs to be corrected for in order to determine u^* and u_{*t} (and u_*' and u_{*t}' in the use of GP88 and MB95). Shao et al. (2011) conveniently reported the parameters necessary to use the shear stress partitioning model of Raupach et al. (1993). This model is considered more physical and less empirical than the model of Marticorena and Bergametti (1995), which we used to correct the Sow et al. (2009) data set (e.g., King et al., 2005). We therefore use the model of Raupach et al. (1993) to obtain the correction factor $f_{\text{eff}} = u_* / u_*' = u_{*t} / u_{*t}'$.

Raupach and colleagues (Raupach, 1992; Raupach et al., 1993) derived an expression for the fraction of the total fluid drag absorbed by the bare soil by first relating the fluid drag absorbed by roughness elements to the frontal area presented to the flow by roughness elements, and then assuming that the area and volume of the wakes of different roughness elements are randomly superimposed. They obtained,

$$f_{\text{eff}}^2 = \frac{u_*^2}{u_*'^2} = \frac{1}{(1 + \beta\lambda)(1 - \sigma\lambda)}. \quad (\text{S.11})$$

Here, β is the ratio of the drag coefficients of a typical roughness element and the bare soil, σ is the ratio of roughness-element basal area to frontal area, and the roughness density λ denotes the frontal area presented to the flow (Marshall, 1971), and is defined as

$$\lambda = nbh, \quad (\text{S.12})$$

where n is the number of roughness elements per unit area, and b and h are the average width and height of the roughness elements. Note that Raupach et al. (1993) also derived a related expression for the ratio of the threshold friction velocity with (u_{*t}') and without (u_{*t}) roughness elements

$$\frac{u_{*t}^2}{u_{*t}^{\prime 2}} = \frac{1}{(1 + m\beta\lambda)(1 - m\sigma\lambda)}. \quad (\text{S.13})$$

Here m ($0 < m \leq 1$) is an empirical parameter meant to account for the fact that the roughness elements produce additional spatial variability in the shear stress exerted on the soil, such that saltation can be initiated at select locations with lower total shear stress than would be denoted by Eq. (S.11). However, the total horizontal sand flux, and thus the vertical dust flux, is determined by the total shear stress exerted on the bare surface. This is described by Eq. (S.11) or, alternatively, by Eq. (S.13) with $m = 1$. We thus use Eq. (S.11) to predict the shear stress partitioning. This is also consistent with the observation by King et al. (2005) that there exists no uniform value of m , such that setting $m = 1$ is reasonable and also results in good agreement with measurements.

Using Eq. (S.11) requires knowledge of the parameters β , λ , and σ . Shao et al. (2011) measured the roughness density $\lambda = 0.02$, and the roughness element basal to frontal area ratio $\sigma = 1$. We further use $\beta = 100$, as recommended by Raupach et al. (1993), which is consistent with field studies of aeolian transport in the presence of roughness elements (Gillette and Stockton, 1989; Lancaster and Baas, 1998; King et al., 2005). Using these parameter values, we find that $f_{\text{eff}} = 0.58 \pm 0.06$ for the Shao et al. (2011) data set, where we estimated from Figure 5 in King et al. (2005) that the relative uncertainty on f_{eff} is $\sim 10\%$.

Note that, for the comparison of the MB95 parameterization with the S111 data set, we compute f_{eff} with the Marticorena and Bergametti (1995) model (Eq. (S.10)), using the soil's aerodynamic roughness length value of $z_0 = 0.48$ mm listed in Shao et al. (2011), yields a value of $f_{\text{eff}} = 0.62 \pm 0.06$. This is consistent with the value of f_{eff} estimated with Eq. (S.11).

5.2.2 Obtaining u_{*t} , α , and C_d

Although the Shao et al. (2011) data set includes many measurements near the threshold, the substantial scatter in these measurements causes their regression against u_* , following the procedure in Appendix B, to not yield a reliable threshold value. Since the Shao et al. (2011) data set contains many measurements near the minimum u_* for wind erosion at the measurement elevation (0.161 m/s), for instance a measurement at $u_* = 0.164$ m/s showing a substantial dust flux of $\sim 200 \mu\text{g}/\text{m}^2/\text{s}$, we take the threshold as $u_{*st} = u_{*st0}$. This is consistent both with the low soil moisture at the site, and with the threshold noted in Shao et al. (2011) of 0.28 m/s without correcting for the presence of erodible roughness elements.

Using the estimated value of u_{*t} , the fragmentation exponent α and dust emission coefficient C_d were estimated through fitting of the dimensionless dust flux as a function of dimensionless friction velocity to Eq. (21) (see Table S1 and Fig. S5i). A second estimate of α was made by fitting Eq. (24) to the measured ratio of the vertical dust flux and the horizontal saltation flux at 5 cm height (see Fig. S6e).

6 The Park et al. (2011) data set (PP11)

Park et al. (2011) made long-term measurements of dust concentration and fluxes at a site north of Naiman in Inner Mongolia, China, at an elevation of 367 m. The site was characterized by shifting, semi-shifting, and fixed dunes, partially covered in low, open shrub (see Fig. 3f). The site was severely affected by desertification. Measurements were made between late fall of 2007 and winter of 2008, during which time the reduction of dust emissions by vegetation was at a minimum. The main dust emission source was to the north and west of the site, and the fetch in

that direction was in excess of 2 km (see Fig. 1c in Park et al. (2011)). The soil texture at the site was sand, with 4% clay, 5% silt, and 91% sand.

6.1 Description of measurements

Park et al. (2011) used a high frequency 3D ultrasonic anemometer, located at 8 m height, to determine the friction velocity directly from the turbulence parameters. The vertical flux of dust was determined by the gradient method (see Appendix C), using measurements of (aerodynamic) PM10 at 3 and 15 m. Park et al. also measured the volumetric soil content at a depth of 5 cm.

6.2 Analysis of data sets

We analyzed the original data sets of wind direction, friction velocity, soil moisture, and vertical dust flux, all of which consisted of averages over 10 minutes. These data comprise a total of 14 dust events, but some of these were due to dust advection from other regions. Since the main dust emission source was to the north and west of the site, we only used events during which the wind direction was between 270° (westerly wind) and 360° (northerly wind), following Park et al. (2011). Furthermore, we exclude events during which the site was snow-covered, events for which negative dust fluxes (deposition) occurred, events for which the threshold could not be reasonably determined, and events for which the scatter in the data overwhelmed the trend of the vertical dust flux with u^* . This procedure excluded all events except for 1 and 2, which respectively occurred on November 19 and 24, 2007. For event 1, the procedure above leaves the data from 10:40 – 20:20 hours, during which time the wind was constant at $327 \pm 15^\circ$ and the vertical dust flux was consistently positive. The friction velocity during this event varied between 0.192 – 1.44 m/s, and the volumetric soil moisture content was $2.8 \pm 0.1 \%$. Similarly, for event 2, we used the data from 9:50 – 22:40 hours, during which time the wind direction was constant at $316 \pm 17^\circ$ and the vertical dust flux was consistently positive. The friction velocity during this event varied between 0.218 – 1.63 m/s, and the volumetric soil moisture was $2.8 \pm 0.1 \%$.

The threshold for Event 1 was determined using the Taylor expansion method at $u_{*t} = 0.171 \pm 0.014$ m/s (see Fig. S4g). For Event 2, there are insufficient data points within 20% of the threshold to determine u_{*t} (see Appendix B). To nonetheless estimate the threshold, we use the 4 data points, the same number as used in the u_{*t} determination for Event 1, taken at the lowest u^* . This yields $u_{*t} = 0.197 \pm 0.016$ (see Fig. S4h).

Using the estimated values of u_{*t} , we estimated the fragmentation exponent α through fitting of the dimensionless dust flux as a function of dimensionless friction velocity to Eq. (21) (see Table S1 and Figs. S5j and S5k). Note that we could not obtain estimates of the dust emission coefficient C_d from the Park et al. (2011) data sets, because the measurement location was not homogeneous due to the presence of extensive dunes and vegetation (see above). In fact, the presence of vegetation at the site makes it surprising that dust emission occurred for relatively low values of the friction velocity. A likely reason for this observation is that the vegetation was not distributed uniformly, allowing the formation of “streets” of unvegetated soil for which the threshold was thus similar to that of a soil with little or no vegetation, as observed by Okin and Gillette (2001) in a similarly vegetated landscape.

Section A: Description of error analysis and least-squares fitting

This supplemental document describes the calculation of uncertainties for the analysis of the compilation of high-quality vertical dust flux data sets. We start by estimating the uncertainty on measurements of u^* and F_d from the literature. Then we discuss the uncertainty in the determination of the soil threshold friction velocity u_{*t} , the fragmentation exponent α , and the dust emission coefficient C_d .

A.1 Uncertainty in the measured quantities u^* and F_d

We use the measured quantities u^* and F_d in our calculations of u_{*t} , α , and C_d for the different data sets. In order to estimate the uncertainty on u_{*t} , α , and C_d , we thus need to estimate the relative uncertainty in these measured quantities, and then propagate them into the uncertainties of u_{*t} , α , and C_d .

The relative error σ_{F_d} / F_d in the vertical dust flux is difficult to assess, but has been shown to be substantial, and following previous studies we take it as 60% (Gillette et al., 1974; Zobeck and Van Pelt, 2006; Fratini et al., 2007). The relative error in u^* from fitting of measured wind profiles to the logarithmic law of the wall (Eq. B.3) was calculated to be ~4% for 15-minute averaging intervals by Namikas et al. (2003). We therefore take the relative error σ_{u^*} / u^* as 0.04, which is a conservative estimate for the 30-minute averaging interval used in this study since the relative error decreases with averaging time (Namikas et al., 2003).

A.1.2 Uncertainty in u_{*t} and u_{*st}

The uncertainty in u_{*t} arises from two main sources: random error due to measurement uncertainty, and systematic error due to the necessarily imperfect procedure for obtaining u_{*t} (see Appendix B). We can calculate the random error from the fitting procedure of Eq. (B.1), which yields a random error varying from ~0.0005 – 0.005 m/s. The random error is therefore likely to be far smaller than the systematic error. Unfortunately, the systematic error is difficult to estimate, but we estimate it as twice the error in u^* . That is, we take $\sigma_{u_{*t}} / u_{*t} = 0.08$.

Another source of error for u_{*t} is the determination of f_{eff} , the correction factor for roughness elements, for the data sets of Sow et al. (2009) and Shao et al. (2011). Note that f_{eff} , and its uncertainty, do not affect the determination of α and C_d , since these parameters are determined through the regression of F_d against u^*/u_{*t} , which is unaffected by f_{eff} . We therefore do not propagate the uncertainty in f_{eff} into $\sigma_{u_{*t}}$. However, the soil's standardized threshold friction velocity u_{*st} , given by Eq. (6), is affected by f_{eff} . Using error propagation (p. 41 of Bevington and Robinson, 2003), the total uncertainty in u_{*st} is

$$\sigma_{u_{*st}} = \sqrt{\frac{\rho_a}{\rho_{a0}} (\sigma_{u_{*t}}^2 + \sigma_{f_{\text{eff}}}^2 u_{*st}^2)}, \quad (\text{A.1})$$

where $\sigma_{f_{\text{eff}}} = 0.1 f_{\text{eff}}$ is the relative error in f_{eff} (see Sections 4.2 and 5.2).

A.2 Non-linear least-squares fitting of dimensionless dust flux and uncertainty in parameters α and C_d

The parameters α and C_d for each data set are obtained through non-linear least squares fitting of the dimensionless dust flux \tilde{F}_d , which is calculated from the measured values of u^* and

F_d as given by Eq. (20). That is, we determine the optimum values of C_d and α by minimizing the goodness-of-fit parameter χ^2 (see p. 142-148 in Bevington and Robinson, 2003),

$$\chi^2 = \sum_i \left[\frac{\tilde{F}_{d,i} - \tilde{F}_d(u_{*,i})}{\sigma_{\tilde{F}_{d,i}}} \right]^2, \quad (\text{A.2})$$

where i sums over all measurements in a given data set, and $\sigma_{\tilde{F}_{d,i}}$ is the uncertainty in the dimensionless dust flux, which we discuss below.

Using error propagation on Eq. (21), the error in the dimensionless dust flux is

$$\sigma_{\tilde{F}_{d,i}}^2 = \sigma_{F_d}^2 \left(\frac{\partial \tilde{F}_{d,i}}{\partial F_{d,i}} \right)^2 + \sigma_{u_*}^2 \left(\frac{\partial \tilde{F}_{d,i}}{\partial u_{*,i}} \right)^2 + \sigma_{u_{*t}}^2 \left(\frac{\partial \tilde{F}_{d,i}}{\partial u_{*t}} \right)^2. \quad (\text{A.3})$$

Using Eq. (20), we have that

$$\frac{\partial \tilde{F}_{d,i}}{\partial F_{d,i}} = \frac{u_{*t}}{f_{\text{bare}} f_{\text{clay}} \sqrt{\rho_a \rho_{a0}} (u_{*,i}^2 - u_{*t}^2)}, \quad (\text{A.4})$$

$$\frac{\partial \tilde{F}_{d,i}}{\partial u_{*,i}} = - \frac{2u_* u_t F_{d,i}}{f_{\text{bare}} f_{\text{clay}} \sqrt{\rho_a \rho_{a0}} (u_{*,i}^2 - u_{*t}^2)^2}, \quad \text{and} \quad (\text{A.5})$$

$$\frac{\partial \tilde{F}_{d,i}}{\partial u_{*t}} = \frac{(u_{*,i}^2 + u_{*t}^2) F_{d,i}}{f_{\text{bare}} f_{\text{clay}} \sqrt{\rho_a \rho_{a0}} (u_{*,i}^2 - u_{*t}^2)^2}. \quad (\text{A.6})$$

Note that we discarded data points with a relative error $\sigma_{\tilde{F}_{d,i}} / \tilde{F}_{d,i}$ in excess of 2, which eliminates approximately 3% of the data points. These data points have u_* very close to u_{*t} , such that $\sigma_{\tilde{F}_{d,i}}$ becomes very large due to the uncertainty in u_{*t} .

A.2.1 Uncertainty in α and C_d

The uncertainty in the parameters α and C_d arising from the fitting procedure is estimated from the values of these parameters at which χ^2 exceeds its minimum value by 1 (see p. 146 in Bevington and Robinson, 2003). For the dust emission coefficient C_d , additional error arises due to the correction factors accounting for differences in fetch length, measured size range, and instrument collection efficiencies. C_d can thus be written as

$$C_d = \hat{C}_d \prod_i f_{\text{corr},i}, \quad (\text{A.7})$$

where \hat{C}_d is the value of C_d that would be obtained without correction factors, Π is the product symbol, and the index i multiplies over the different correction factors $f_{\text{corr},i}$. Using error propagation, the relative uncertainty in C_d is then

$$\frac{\sigma_{C_d}}{C_d} = \sqrt{\frac{\sigma_{\hat{C}_d}^2}{\hat{C}_d^2} + \sum_i \frac{\sigma_{f_{\text{corr},i}}^2}{f_{\text{corr},i}^2}}, \quad (\text{A.8})$$

where $\sigma_{\hat{C}_d}$ is obtained from the fitting procedure as described above, and $\sigma_{f_{\text{corr},i}}$ denotes the error due to each correction factor. Note that this calculation of the uncertainty in C_d does not include possible systematic errors arising from the measurements of the dust concentration or wind speed.

A.3 Linear least-squares fitting of sandblasting efficiency and resulting uncertainty in α

In addition to obtaining the fragmentation exponent α from the dimensionless dust flux using the procedure described above, we also obtain an estimate of α by fitting the sandblasting efficiency to Eq. (24) for those data sets that also measured the saltation (impact) flux. This equation can be cast in the form

$$y = a + bx, \quad (\text{A.9})$$

where $x = \ln(u_*)$, $y = \ln(F_d / Q_d)$, $a = \ln(C_s)$, and $b = \alpha - r$. We then calculate the intercept a and slope b using standard linear least squares analysis assuming that the uncertainty is equal for each data point (p. 98-115 in Bevington and Robinson, 2003). We then obtain the value of the fragmentation exponent and its uncertainty as follows

$$\alpha = b + r, \text{ and} \quad (\text{A.10})$$

$$\sigma_\alpha^2 = \sigma_b^2 + \sigma_r^2, \quad (\text{A.11})$$

where σ_b is the uncertainty in the slope b obtained from the linear least squares fit, and we take $\sigma_r = 0.50$ (see Section 3.3 in the main text).

A.4 Linear least-squares fitting of C_α , C_{d0} , and C_e and resulting uncertainties

A.4.1 The parameters C_e and C_{d0}

As described in the main text, the dimensionless parameters C_{d0} and C_e are derived from the linear least-squares fit of α as a function of u_{*st} , using Eq. (18). That is, we cast Eq. (18) into the form of Eq. (A.9), with $x = (u_{*st} - u_{*st0})/u_{*st0}$, $y = \ln(C_d)$, $a = \ln(C_{d0})$, and $b = -C_e$. However, unlike for the measurements of the sandblasting efficiency, the errors on the individual C_d data points are not equal, which complicates the least-squared fit somewhat. For this case of unequal errors, the values of a , b , σ_a , and σ_b are given by (p. 98-115 in Bevington and Robinson (2003))

$$a = \frac{1}{\Delta'} \left(\sum_i \frac{x_i^2}{\sigma_{y,i}^2} \sum_i \frac{y}{\sigma_y^2} - \sum_i \frac{x_i}{\sigma_{y,i}^2} \sum_i \frac{y_i x_i}{\sigma_{y,i}^2} \right), \quad (\text{A.12})$$

$$b = \frac{1}{\Delta'} \left(\sum_i \frac{1}{\sigma_{y,i}^2} \sum_i \frac{y_i x_i}{y_i^2} - \sum_i \frac{x_i}{\sigma_{y,i}^2} \sum_i \frac{y_i}{\sigma_{y,i}^2} \right), \quad (\text{A.13})$$

$$\sigma_a^2 = \frac{1}{\Delta} \sum_i \frac{x_i^2}{\sigma_{y,i}^2}, \quad (\text{A.14})$$

$$\sigma_b^2 = \frac{1}{\Delta} \sum_i \frac{1}{\sigma_{y,i}^2}, \text{ with} \quad (\text{A.15})$$

$$\Delta = \sum_i \frac{1}{\sigma_{y,i}^2} \sum_i \frac{x_i^2}{\sigma_{y,i}^2} - \left(\sum_i \frac{x_i}{\sigma_{y,i}^2} \right)^2. \quad (\text{A.16})$$

Note that uncertainty in the fit arises from uncertainty in both the dependent and independent variables. We thus propagate the uncertainty in the independent variable, $x = (u_{*st} - u_{*t0})/u_{*t0}$ in this case, into the dependent variable, $y = \ln(C_d)$. We do this following p. 102 in Bevington and Robinson,

$$\sigma_{y,i}^2 = \sigma_{yl,i}^2 + \sigma_{yD,i}^2, \quad (\text{A.17})$$

where $\sigma_{yD,i}$ is the ‘regular’ uncertainty in the dependent variable, and $\sigma_{yI,i}$ is the uncertainty arising from uncertainty in the independent variable, which equals

$$\sigma_{yI,i} = \sigma_{x,i} \frac{dy}{dx}. \quad (\text{A.18})$$

We determine the slope dy/dx from a linear fit to the data using only the ‘regular’ y -uncertainty, and then use dy/dx to calculate the total uncertainty on each data point using Eqs. (A.17) and (A.18). This uncertainty is then used to determine the least-squares fit and its uncertainty following the procedure above.

The uncertainty σ_{fit} at a given point on the fitted line can be derived from error propagation of Eq. (A.9),

$$\sigma_{\text{fit}} = \sqrt{\sigma_a^2 \left(\frac{\partial y}{\partial a} \right)^2 + \sigma_b^2 \left(\frac{\partial y}{\partial b} \right)^2 + 2\sigma_{ab}^2 \left(\frac{\partial y}{\partial a} \right) \left(\frac{\partial y}{\partial b} \right)} = \sqrt{\sigma_a^2 + \sigma_b^2 x^2 + 2\sigma_{ab}^2 x} \quad (\text{A.19})$$

where the covariance σ_{ab}^2 is defined as (p. 123 in Bevington and Robinson, 2003)

$$\sigma_{ab}^2 = \sum_i \sigma_{y,i}^2 \frac{\partial a}{\partial y_i} \frac{\partial b}{\partial y_i}. \quad (\text{A.20})$$

The partial derivatives in Eq. (A.20) quantify the sensitivity of the parameters a and b to the value y_i of each individual measurement. These partial derivatives are defined as (p. 109 in Bevington and Robinson, 2003)

$$\frac{\partial a}{\partial y_j} = \frac{1}{\Delta \sigma_{y,j}^2} \left(\sum_i \frac{x_i^2}{\sigma_{y,i}^2} - x_j \sum_i \frac{x_i}{\sigma_{y,i}^2} \right), \text{ and} \quad (\text{A.21})$$

$$\frac{\partial b}{\partial y_j} = \frac{1}{\Delta \sigma_{y,j}^2} \left(x_j \sum_i \frac{1}{\sigma_{y,i}^2} - \sum_i \frac{x_i}{\sigma_{y,i}^2} \right), \quad (\text{A.22})$$

where both i and j sum over all measurements in a given data set.

A.4.2 The parameter C_α and its uncertainty

As described in the main text, the dimensionless parameter C_α is derived from the linear least-squares fit of α as a function of u_{*st} using Eq. (18a). That is, we obtain C_α by minimizing the goodness-of-fit parameter χ^2 (see p. 142-148 in Bevington and Robinson, 2003)

$$\chi^2 = \sum_i \left[\frac{\alpha_i - C_\alpha (u_{*st} - u_{*st0}) / u_{*st0}}{\sigma_{\alpha,i}} \right]^2, \quad (\text{A.23})$$

where we obtain σ_{C_α} from the values of C_α at which χ^2 exceeds its minimum value by 1 (see p. 146 in Bevington and Robinson, 2003). The uncertainty σ_{fit} at a given point on the fitted line is obtained using Eq. (A.19), which yields

$$\sigma_{\text{fit}} = \sigma_{C_\alpha} (u_{*st} - u_{*st0}) / u_{*st0}.$$

A.5 Uncertainty in the parameterized vertical dust flux

The main article uses parameterizations to predict the vertical dust flux for measured values of u^* and u_{*t} . However, these measured values are uncertain, and this uncertainty affects the theoretical predictions. To make an accurate comparison between measured and predicted values of the vertical dust flux, the experimental uncertainty in u^* and u_{*t} must thus be propagated into

the theoretical predictions. Following standard error propagation, we calculate this theoretical error as

$$\sigma_{F_{d,i}}^2 = \sigma_{u_{*,i}}^2 \left(\frac{\partial F_{d,i}}{\partial u_{*,i}} \right)^2 + \sigma_{u_{*,t}}^2 \left(\frac{\partial F_{d,i}}{\partial u_{*,t}} \right)^2, \quad (\text{A.24})$$

where $F_{d,i}$ is the theoretical prediction of a given parameterization for data point i . The derivatives in Eq. (A.24) are obtained from the respective parameterizations. For the parameterizations of Gillette and Passi (1988) and Marticorena and Bergametti (1995) this yields, respectively,

$$\sigma_{GP,i}^2 = C_{GP} f_{bare} u_{*,i}^2 \left\{ \sigma_{u_{*,i}}^2 [4u_{*,i} - 3u_{*,t}]^2 + \sigma_{u_{*,t}}^2 u_{*,i}^2 \right\}^{1/2}, \text{ and} \quad (\text{A.25})$$

$$\sigma_{MB,i}^2 = \frac{C_{MB} f_{bare} \rho_a (u_{*,i} + u_{*,t})}{g} \left[\sigma_{u_{*,i}}^2 (3u_{*,i} - u_{*,t})^2 + \sigma_{u_{*,t}}^2 (u_{*,i} - 3u_{*,t})^2 \right]^{1/2}. \quad (\text{A.26})$$

The expression for the uncertainty in the vertical dust flux predicted by the present parameterization is more involved, with the derivatives in Eq. (18) given by,

$$\frac{\partial F_{d,i}}{\partial u_{*,i}} = \frac{f_{bare} f_{clay} \rho_a C_{d0}}{u_{*,i} u_{*,st0} u_{*,st}} \exp\left(-C_e \frac{u_{*,st} - u_{*,st0}}{u_{*,st0}}\right) \left(\frac{u_{*,i}}{u_{*,t}}\right)^{C_a \frac{u_{*,st} - u_{*,st0}}{u_{*,st0}}} \left[2u_{*,i}^2 u_{*,st0} + C_a (u_{*,i}^2 - u_{*,t}^2) (u_{*,st} - u_{*,st0}) \right], \quad (\text{A.27})$$

$$\begin{aligned} \frac{\partial F_{d,i}}{\partial u_{*,st}} = & \frac{f_{bare} f_{clay} \rho_a C_{d0}}{u_{*,st0} u_{*,st}^2} \exp\left(-C_e \frac{u_{*,st} - u_{*,st0}}{u_{*,st0}}\right) \left(\frac{u_{*,i}}{u_{*,t}}\right)^{C_a \frac{u_{*,st} - u_{*,st0}}{u_{*,st0}}} \left\{ C_a u_{*,st} (u_{*,i}^2 - u_{*,st}^2) \ln\left(\frac{u_{*,i}}{u_{*,t}}\right) + \right. \\ & \left. - (u_{*,i}^2 - u_{*,t}^2) [C_a (u_{*,st} - u_{*,st0}) + C_e u_{*,st}] - (u_{*,i}^2 + u_{*,t}^2) u_{*,st0} \right\}. \end{aligned} \quad (\text{A.28})$$

Section B: Estimating the bare soil threshold friction velocity of literature data sets

A critical part of our analysis procedure is estimating the threshold friction velocity u_{*t} above which dust emission occurs for each data set. As discussed in the main article, this theoretical definition of a threshold u_* is not fully consistent with the reality in the field, since there is no clear value of u_* above which dust emission does and below which it does not occur (Wiggs et al., 2004). Considering this limitation, we obtain u_{*t} in a manner that is most consistent with its theoretical definition in both Sections 2.1 and 2.2 and in previous studies (Gillette and Passi, 1988; Shao and Raupach, 1993; Marticorena and Bergametti, 1995). That is, we define u_{*t} as the value of u_* at which the vertical dust flux, when regressed against measurements at values of u_* close to the threshold, equal zero.

Since dust emission results predominantly from saltation bombardment (Gillette et al., 1974; Shao and Raupach, 1993), and since measuring the saltation flux is substantially simpler than measuring the dust flux, an accurate way of estimating the dust emission threshold is to estimate the saltation threshold from saltation flux measurements. We therefore follow previous studies (Gillette et al., 1997; Clifton et al., 2006; Barchyn and Hugenholtz, 2011), and estimate u_{*t} by using a Taylor expansion around $u_* \approx u_{*t}$ to approximate the saltation flux Q . For the data sets for which no saltation flux measurements are available (i.e., GB04, FC07, and PP11), we instead use a Taylor expansion for the dust flux F_d . Specifically, we use a 2nd-order Taylor expansion, yielding

$$Q \approx c_{Q_{\text{tay}}} (u_*^2 - u_{*t}^2), \text{ and} \quad (\text{B.1})$$

$$F_d \approx c_{F_{\text{tay}}} (u_*^2 - u_{*t}^2). \quad (\text{B.2})$$

where $c_{F_{\text{tay}}}$ and $c_{Q_{\text{tay}}}$ are proportionality constants. The error of the approximation of Eq. (B.1) relative to Eqs. (22, 23) for Q is $< 2\%$ for $u_*/u_{*t} \leq 1.20$ and $0 \leq r \leq 1$. Similarly, the error of the approximation Eq. (B.2) relative to Eq. (18) for F_d is $< 17\%$ for $u_*/u_{*t} \leq 1.20$ and $0 \leq a \leq 4$. Since these errors are small relative to the total uncertainty in F_d (see Appendix A.1), we obtain u_{*t} for each data set by iteratively fitting Eqs. (B.1, B.2) to measurements for which $u_*/u_{*t} \leq 1.20$.

Figures of the determination of u_{*t} for all data sets for which we used the Taylor expansion method are presented in Fig. S4. Note that the Taylor expansion method was unable to produce a reliable estimate of u_{*t} for some data sets, either because there were not enough measurements near the threshold (in the case of FC07), or because the data were too scattered (in the case of SI11). However, the dust emission threshold for these cases is very close to the minimal threshold u_{*st0} , such that a reasonable value for u_{*st} can be inferred.

Some previous studies have used the alternative Time Fraction Equivalence Method (TFEM) (Stout and Zobeck, 1997; Wiggs et al., 2004), which derives a threshold wind speed by calculating the fraction of measurement intervals (typically 1 second or 1 minute) during which saltation occurs. We do not use this method here for two reasons. First, only some of the data sets measured the saltation flux and the TFEM method can thus be used only for a portion of the data set, introducing systematic error in the determination of u_{*t} between the data sets because of the use of different methods (Barchyn and Hugenholtz, 2011). Second, the friction velocity u_* is meaningful only for averaging times sufficiently long to access the lower-frequency components of the boundary layer turbulence, requiring averaging times in excess of ~ 10 minutes (Kaimal and Finnigan, 1994; van Boxel et al., 2004). Therefore, the theoretical definition of u_{*t} is meaningful only on timescales in excess of ~ 10 minutes, such that a determination of u_{*t} with the TFEM method, which is done with substantially higher temporal resolution (~ 1 second or minute) saltation data, would be inconsistent.

Section C: Inferring the vertical dust flux from measured dust concentration profiles

Most studies in our high-quality dust flux measurements compilation (i.e., ZP06, SA09, SII1, and PP11) calculated the vertical dust flux by combining measurements of the vertical wind profile with measurements of the vertical concentration profile, using the gradient method first proposed by Gillette et al. (1972). The only exception is the study of Fratini et al. (2007), who used eddy covariance to determine the dust flux. For the GB04 and ZP06 data sets, we obtained the original vertical concentration profile and wind profile data. We then used these measurements to calculate the vertical dust flux as follows.

Since $\leq 10 \mu\text{m}$ geometric diameter dust has a small settling velocity compared to turbulent fluctuations in vertical wind speed, we assume it to be a passive tracer (Gillette et al., 1972; Fratini et al., 2007). In the atmospheric boundary layer, passive tracers are predominantly transported by turbulent eddies. In analogy with, for instance, the mixing of horizontal fluid momentum, we can write (Gillette et al., 1972)

$$F_d = -K_d \frac{\partial c}{\partial z}, \quad (\text{C.1})$$

where F_d ($\text{kg}/\text{m}^2/\text{s}$) is the vertical flux of dust, c (kg/m^3) is the mass concentration of dust aerosols at height z , and K_d (m^2/s) is the turbulent diffusivity. Assuming that the transfer of dust aerosols is similar to that of fluid momentum (Gillette et al., 1972), and using mixing length theory (Prandtl, 1925), we have

$$K_d = \eta \kappa u_* z. \quad (\text{C.2})$$

where η is the ratio of the dust and momentum turbulent diffusivities and is of order unity, and $\kappa \approx 0.40$ is von Kármán's constant. The friction velocity u_* can be derived from the wind profile using the "law of the wall" (Prandtl, 1935),

$$U(z) = \frac{u_*}{\kappa} \ln\left(\frac{z}{z_0}\right), \quad (\text{C.3})$$

where U is the wind speed averaged over a sufficiently long interval, usually at least 10 minutes (Kaimal and Finnigan, 1994; van Boxel et al., 2004), and z_0 is the aerodynamic roughness of the surface.

Since the dust flux can be assumed constant in the surface layer (Shao, 2008), we have from Eq. (C.1) that the concentration gradient scales with the inverse height, and that the concentration profile must consequently be logarithmic. Monin (Monin, 1970) similarly argued that the concentration profile of passive tracers such as humidity must be logarithmic. Furthermore, Kind (Kind, 1992) showed that, in the case of horizontal homogeneity of the surface and stationary, isotropic turbulence, the concentration profile of passive tracers should follow

$$\frac{c(z)}{c_r} = 1 - \frac{F_d}{\kappa u_* c_r} \ln\left(\frac{z}{z_r}\right), \quad (\text{C.4})$$

Where c is the tracer's concentration, and c_r is the concentration at the reference height z_r . Gillies and Berkofsky (2004) found that this logarithmic profile fit measured dust concentration profiles during surface emission better than previously proposed power law concentration profiles (Anderson and Hallet, 1986). For a given measured concentration profile at a certain value of u_* and c_r , we then obtain the dust flux F_d from the regression of c/c_r against $\ln(z/z_r)$.

Note that for the situation of only 2 measurement heights, Eq. (C.4) reduces to the gradient method proposed by Gillette et al. (1972) and used by, e.g., Sow et al. (2009), Shao et al. (2011), and Park et al. (2011). That is,

$$F_d = \kappa u_* \frac{(c_1 - c_2)}{\ln(z_1 / z_2)}, \quad (\text{C.5})$$

where c_1 , z_1 , c_2 , and z_2 refer to the dust concentration and height at the two measurement locations.

References

- Anderson, R. S. and Hallet, B.: Sediment transport by wind - toward a general-model, *Geol. Soc. Am. Bull.*, 97, 523-535, 1986.
- Barchyn, T. E. and Hugenholtz, C. H.: Comparison of four methods to calculate aeolian sediment transport threshold from field data: Implications for transport prediction and discussion of method evolution, *Geomorphology*, 129, 190-203, 2011.
- Bevington, P. R. and Robinson, D. K.: *Data reduction and error analysis*, McGraw-Hill, New York, 2003.
- Clifton, A., Ruedi, J. D., and Lehning, M.: Snow saltation threshold measurements in a drifting-snow wind tunnel, *Journal of Glaciology*, 52, 585-596, 2006.
- Creyssels, M., Dupont, P., El Moctar, A. O., Valance, A., Cantat, I., Jenkins, J. T., Pasini, J. M., and Rasmussen, K. R.: Saltating particles in a turbulent boundary layer: experiment and theory, *Journal of Fluid Mechanics*, 625, 47-74, 2009.
- FAO: *Harmonized World Soil Database (version 1.2)*, FAO, Rome, Italy and IIASA, Laxenburg, Austria, 2012.
- Fecan, F., Marticorena, B., and Bergametti, G.: Parametrization of the increase of the aeolian erosion threshold wind friction velocity due to soil moisture for arid and semi-arid areas, *Ann Geophys-Atm Hydr*, 17, 149-157, 1999.
- Fratini, G., Ciccioli, P., Febo, A., Forgiione, A., and Valentini, R.: Size-segregated fluxes of mineral dust from a desert area of northern China by eddy covariance, *Atmospheric Chemistry and Physics*, 7, 2839-2854, 2007.
- Fratini, G., Santini, M., Ciccioli, P., and Valentini, R.: Evaluation of a wind erosion model in a desert area of northern Asia by eddy covariance, *Earth Surface Processes and Landforms*, 34, 1743-1757, 2009.
- Gillette, D. A.: On the production of soil wind erosion having the potential for long range transport, *J. Rech. Atmos.*, 8, 734-744, 1974.
- Gillette, D. A., Blifford, I. H., and Fenster, C. R.: Measurements of aerosol size distributions and vertical fluxes of aerosols on land subject to wind erosion, *J. Appl. Meteor.*, 11, 977-987, 1972.
- Gillette, D. A., Blifford, I. H., and Fryrear, D. W.: Influence of wind velocity on size distributions of aerosols generated by wind erosion of soils, *Journal of Geophysical Research*, 79, 4068-4075, 1974.
- Gillette, D. A., Fryrear, D. W., Xiao, J. B., Stockton, P., Ono, D., Helm, P. J., Gill, T. E., and Ley, T.: Large-scale variability of wind erosion mass flux rates at Omens Lake .1. Vertical profiles of horizontal mass fluxes of wind-eroded particles with diameter greater than 50 μ m, *Journal of Geophysical Research-Atmospheres*, 102, 25977-25987, 1997.
- Gillette, D. A. and Passi, R.: Modeling dust emission caused by wind erosion, *Journal of Geophysical Research-Atmospheres*, 93, 14233-14242, 1988.
- Gillette, D. A. and Stockton, P. H.: The effect of nonerodible particles on wind erosion of erodible surfaces, *Journal of Geophysical Research-Atmospheres*, 94, 12885-12893, 1989.
- Gillies, J. A. and Berkofsky, L.: Eolian suspension above the saltation layer, the concentration profile, *Journal of Sedimentary Research*, 74, 176-183, 2004.
- Greeley, R. and Iversen, J. D.: *Wind as a Geological Process on Earth, Mars, Venus, and Titan*. Cambridge Univ. Press., New York, 1985.
- Ho, T. D., Valance, A., Dupont, P., and El Moctar, A. O.: Scaling Laws in Aeolian Sand Transport, *Phys. Rev. Lett.*, 106, 2011.

- Houser, C. A. and Nickling, W. G.: The factors influencing the abrasion efficiency of saltating grains on a clay-crusting playa, *Earth Surface Processes and Landforms*, 26, 491-505, 2001.
- Ishizuka, M., Mikami, M., Leys, J., Yamada, Y., Heidenreich, S., Shao, Y., and McTainsh, G. H.: Effects of soil moisture and dried raindrop crust on saltation and dust emission, *Journal of Geophysical Research-Atmospheres*, 113, 2008.
- Ishizuka, M., Mikami, M., Leys, J. F., Shao, Y., Yamada, Y., and Heidenreich, S.: Power law relation between size-resolved vertical dust flux and friction velocity measured in a fallow wheat field, *Aeolian Research*, in press, 2014.
- Kaaden, N., Massling, A., Schladitz, A., Muller, T., Kandler, K., Schutz, L., Weinzierl, B., Petzold, A., Tesche, M., Leinert, S., Deutscher, C., Ebert, M., Weinbruch, S., and Wiedensohler, A.: State of mixing, shape factor, number size distribution, and hygroscopic growth of the Saharan anthropogenic and mineral dust aerosol at Tinfou, Morocco, *Tellus Ser. B-Chem. Phys. Meteorol.*, 61, 51-63, 2009.
- Kaimal, J. C. and Finnigan, J. J.: *Atmospheric boundary layer flows: Their structure and measurement* Oxford Univ. Press, New York, 1994.
- Kind, R. J.: One-dimensional aeolian suspension above beds of loose particles - a new concentration-profile equation, *Atmospheric Environment Part a-General Topics*, 26, 927-931, 1992.
- King, J., Nickling, W. G., and Gillies, J. A.: Representation of vegetation and other nonerodible elements in aeolian shear stress partitioning models for predicting transport threshold, *Journal of Geophysical Research-Earth Surface*, 110, 2005.
- Kok, J. F.: Difference in the Wind Speeds Required for Initiation versus Continuation of Sand Transport on Mars: Implications for Dunes and Dust Storms, *Phys. Rev. Lett.*, 104, 074502, 2010a.
- Kok, J. F.: An improved parameterization of wind-blown sand flux on Mars that includes the effect of hysteresis, *Geophysical Research Letters*, 37, 2010b.
- Kok, J. F., Parteli, E. J. R., Michaels, T. I., and Karam, D. B.: The physics of wind-blown sand and dust, *Reports on Progress in Physics*, 75, 106901, 2012.
- Kok, J. F. and Renno, N. O.: A comprehensive numerical model of steady state saltation (COMSALT), *Journal of Geophysical Research-Atmospheres*, 114, D17204, 2009.
- Lancaster, N. and Baas, A.: Influence of vegetation cover on sand transport by wind: Field studies at Owens Lake, California, *Earth Surface Processes and Landforms*, 23, 69-82, 1998.
- Marshall, J. K.: Drag measurements in roughness arrays of varying density and distribution, *Agricultural Meteorology*, 8, 269-&, 1971.
- Marticorena, B. and Bergametti, G.: Modeling the atmospheric dust cycle .1. Design of a soil-derived emission scheme, *Journal of Geophysical Research-Atmospheres*, 100, 16415-16430, 1995.
- Monin, A. S.: Atmospheric boundary layer, *Annual Review of Fluid Mechanics*, 2, 225-250, 1970.
- Namikas, S. L., Bauer, B. O., and Sherman, D. J.: Influence of averaging interval on shear velocity estimates for aeolian transport modeling, *Geomorphology*, 53, 235-246, 2003.
- Owen, P. R.: Saltation of uniform grains in air, *Journal of Fluid Mechanics*, 20, 225-242, 1964.
- Park, M. S., Park, S. U., and Chun, Y.: Improved parameterization of dust emission (PM10) fluxes by the gradient method using the Naiman tower data at the Horqin desert in China, *Science of the Total Environment*, 412, 265-277, 2011.

- Prandtl, L.: Bericht uber Untersuchungen zur ausgebildeten Turbulenz, *Z. angew. Math. Mech.*, 5, 136-139, 1925.
- Prandtl, L.: The mechanics of viscous flows. In: *Aerodynamic Theory*, Durand, W. F. (Ed.), Springer, Berlin, 1935.
- Rajot, J. L., Formenti, P., Alfaro, S., Desboeufs, K., Chevaillier, S., Chatenet, B., Gaudichet, A., Journet, E., Marticorena, B., Triquet, S., Maman, A., Mouget, N., and Zakou, A.: AMMA dust experiment: An overview of measurements performed during the dry season special observation period (SOP0) at the Banizoumbou (Niger) supersite, *Journal of Geophysical Research-Atmospheres*, 113, 2008.
- Rasmussen, K. R. and Sorensen, M.: Vertical variation of particle speed and flux density in aeolian saltation: Measurement and modeling, *Journal of Geophysical Research-Earth Surface*, 113, 2008.
- Raupach, M. R.: Drag and drag partition on rough surfaces, *Boundary-Layer Meteorology*, 60, 375-395, 1992.
- Raupach, M. R., Gillette, D. A., and Leys, J. F.: The effect of roughness elements on wind erosion threshold, *Journal of Geophysical Research-Atmospheres*, 98, 3023-3029, 1993.
- Schuepp, P. H., Leclerc, M. Y., Macpherson, J. I., and Desjardins, R. L.: Footprint prediction of scalar fluxes from analytical solutions of the diffusion equation, *Boundary-Layer Meteorology*, 50, 353-373, 1990.
- Shao, Y., Ishizuka, M., Mikami, M., and Leys, J. F.: Parameterization of size-resolved dust emission and validation with measurements, *Journal of Geophysical Research-Atmospheres*, 116, D08203, 2011.
- Shao, Y. and Raupach, M. R.: Effect of saltation bombardment on the entrainment of dust by wind, *J. Geophys. Res.*, 98, 12719-12726, 1993.
- Shao, Y. P.: *Physics and Modelling of Wind Erosion*, Springer, Heidelberg, 2008.
- Sherman, D. J.: An equilibrium relationship for shear velocity and apparent roughness length in aeolian saltation, *Geomorphology*, 5, 419-431, 1992.
- Sow, M.: *Mesure, caractérisation et paramétrisation des flux d'aérosols terrigènes produits par érosion éolienne en zone sahélienne*, 2009. Université Paris XII, 2009.
- Sow, M., Alfaro, S. C., Rajot, J. L., and Marticorena, B.: Size resolved dust emission fluxes measured in Niger during 3 dust storms of the AMMA experiment, *Atmospheric Chemistry and Physics*, 9, 3881-3891, 2009.
- Spaan, W. P. and van den Abeele, G. D.: Wind borne particle measurements with acoustic sensors, *Soil Technology*, 4, 51-63, 1991.
- Stockton, P. H. and Gillette, D. A.: Field measurement of the sheltering effect of vegetation on erodible land surfaces, *Land Degradation & Rehabilitation*, 2, 77-85, 1990.
- Stout, J. E. and Zobeck, T. M.: Intermittent saltation, *Sedimentology*, 44, 959-970, 1997.
- TSI Inc.: *DustTrak™ DRX aerosol monitor calibration methods*, 2012.
- van Boxel, J. H., Sterk, G., and Arens, S. M.: Sonic anemometers in aeolian sediment transport research, *Geomorphology*, 59, 131-147, 2004.
- Wang, X. L., Chancellor, G., Evenstad, J., Farnsworth, J. E., Hase, A., Olson, G. M., Sreenath, A., and Agarwal, J. K.: A Novel Optical Instrument for Estimating Size Segregated Aerosol Mass Concentration in Real Time, *Aerosol Science and Technology*, 43, 939-950, 2009.
- Wiggs, G. F. S., Atherton, R. J., and Baird, A. J.: Thresholds of aeolian sand transport: establishing suitable values, *Sedimentology*, 51, 95-108, 2004.

- Yamada, Y., Mikami, M., and Nagashima, H.: Dust particle measuring system for streamwise dust flux, *Journal of Arid Land Studies*, 11, 229-234, 2002.
- Zobeck, T. M. and Van Pelt, R. S.: Wind-induced dust generation and transport mechanics on a bare agricultural field, *Journal of Hazardous Materials*, 132, 26-38, 2006.

Supplementary Tables

Table S1. Main results of the analysis of the quality-controlled compilation of vertical dust flux data sets.

Study	Event	Estimated u_{*in} (m/s)	α from fit to F_d	α from fit to F_d/Q	C_d ($\times 10^{-6}$)
GB04	Feb 16	0.23 ± 0.02	1.6 ± 0.5	-	3.9 ± 1.3
GB04	March 20	0.29 ± 0.02	1.6 ± 0.5	-	10 ± 3
ZP06	March 4	0.39 ± 0.03	3.4 ± 2.4	5.3 ± 1.4	2.0 ± 1.2
ZP06	March 18	0.35 ± 0.06	3.3 ± 1.0	2.4 ± 0.7	5.7 ± 3.1
FC07	Event 1	0.192 ± 0.015	0.2 ± 0.2	-	-
FC07	Event 2	0.161 ± 0.013	-0.4 ± 0.2	-	-
SA09	ME1	0.233 ± 0.030	2.0 ± 0.7	1.7 ± 0.5	41 ± 14
SA09	CE4	0.228 ± 0.029	3.0 ± 0.6	2.6 ± 0.8	35 ± 13
SI11	N/A	0.160 ± 0.021	0.5 ± 0.4	0.5 ± 0.5	45 ± 5
PP11	Event 1	0.167 ± 0.013	-0.1 ± 0.2	-	-
PP11	Event 2	0.193 ± 0.015	0.1 ± 0.2	-	-

Supplementary Figures

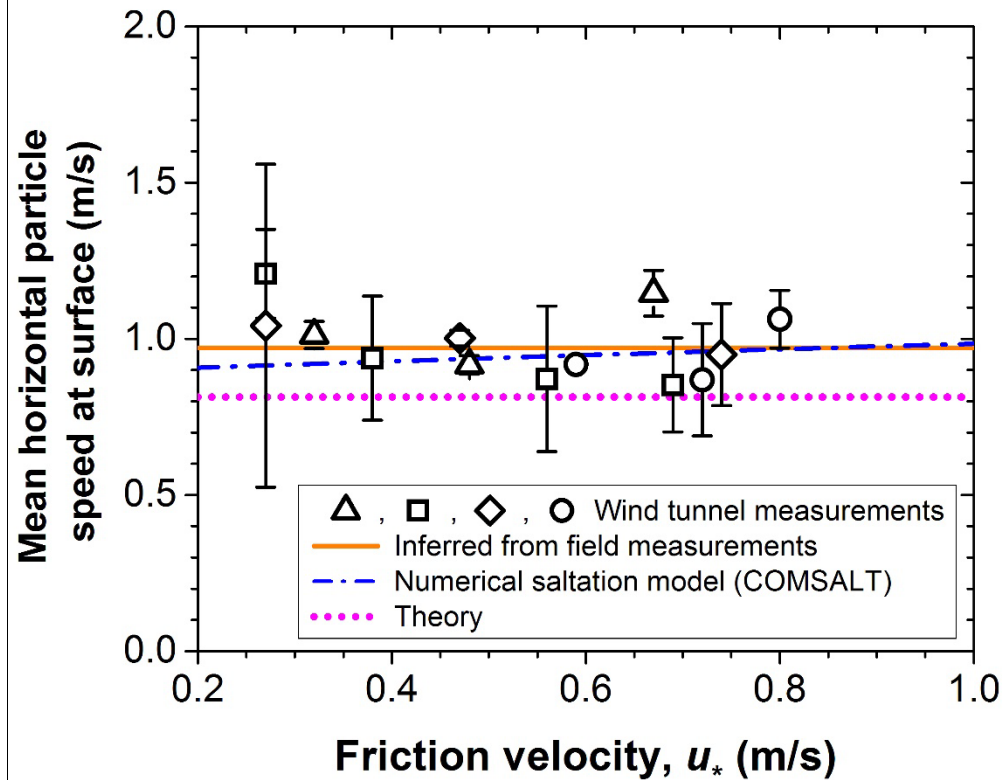


Figure S1. Wind tunnel measurements of the speed of $\sim 250 - 300 \mu\text{m}$ saltions (symbols) indicate that the mean horizontal speed at the surface stays constant with u_* . Similarly, Namikas (2003) inferred from his field measurements that the speed at which saltions are launched from the surface is independent of u_* (solid orange line). Also included are simulations with the numerical model COMSALT (Kok and Renno, 2009) (dash-dotted blue line), and the prediction of the theory of Kok (2010b) (dotted magenta line). (Estimates of the surface particle speed in the wind tunnel measurements of Rasmussen and Sorensen (2008) (squares and diamonds denote measurements with 242 and $320 \mu\text{m}$ sand, respectively), Creyssels et al. (2009) (triangles, $242 \mu\text{m}$ sand), and Ho et al. (2011) (circles, $230 \mu\text{m}$ sand) were obtained by linearly extrapolating horizontal particle speed measurements within 2 mm of the surface (see Kok (2010a). Error bars were derived from the uncertainty in the fitting parameters.) After Kok et al. (2012).

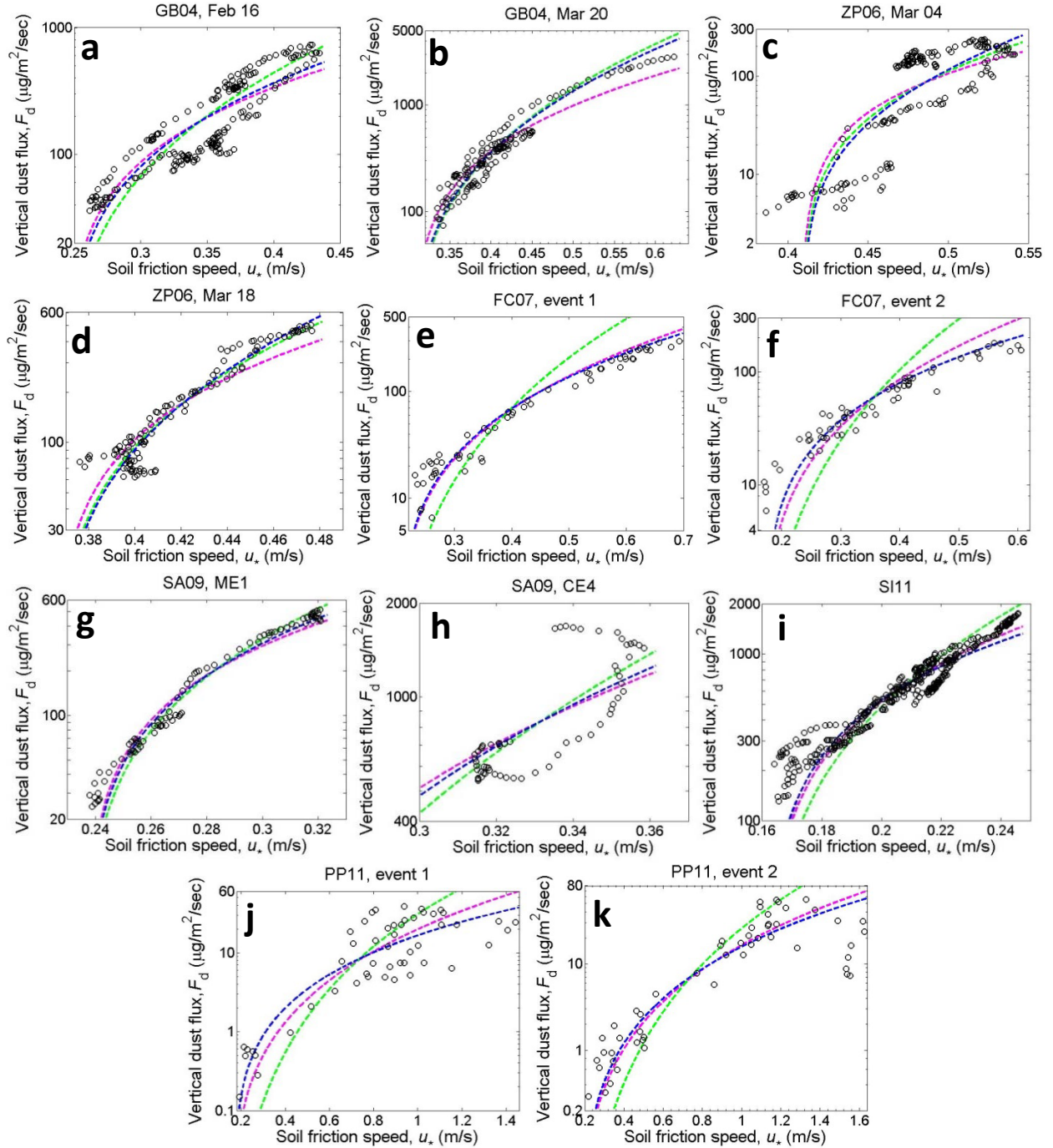


Figure S2. The vertical dust flux F_d as a function of the soil friction velocity u_* for each of the 11 data sets. Plotted for comparison are the dust fluxes predicted by GP88 (green lines), MB95 (magenta lines), and this study (Eq. 18; blue lines). To facilitate comparison of the functional forms of these parameterizations with the data, the proportionality constant in all three parameterizations was tuned to produce maximum agreement with each data set. Since the SA09 and S11 data sets contained roughness elements, the friction velocity u_*' that is used in MB95 differed from the soil friction velocity u_* used in GP88 and Eq. (18). To nonetheless plot the predictions of the three schemes on one graph, we thus converted measured values of u_*' to u_* following the drag partition methods discussed in Sections 4.2.1 and 5.2.1.

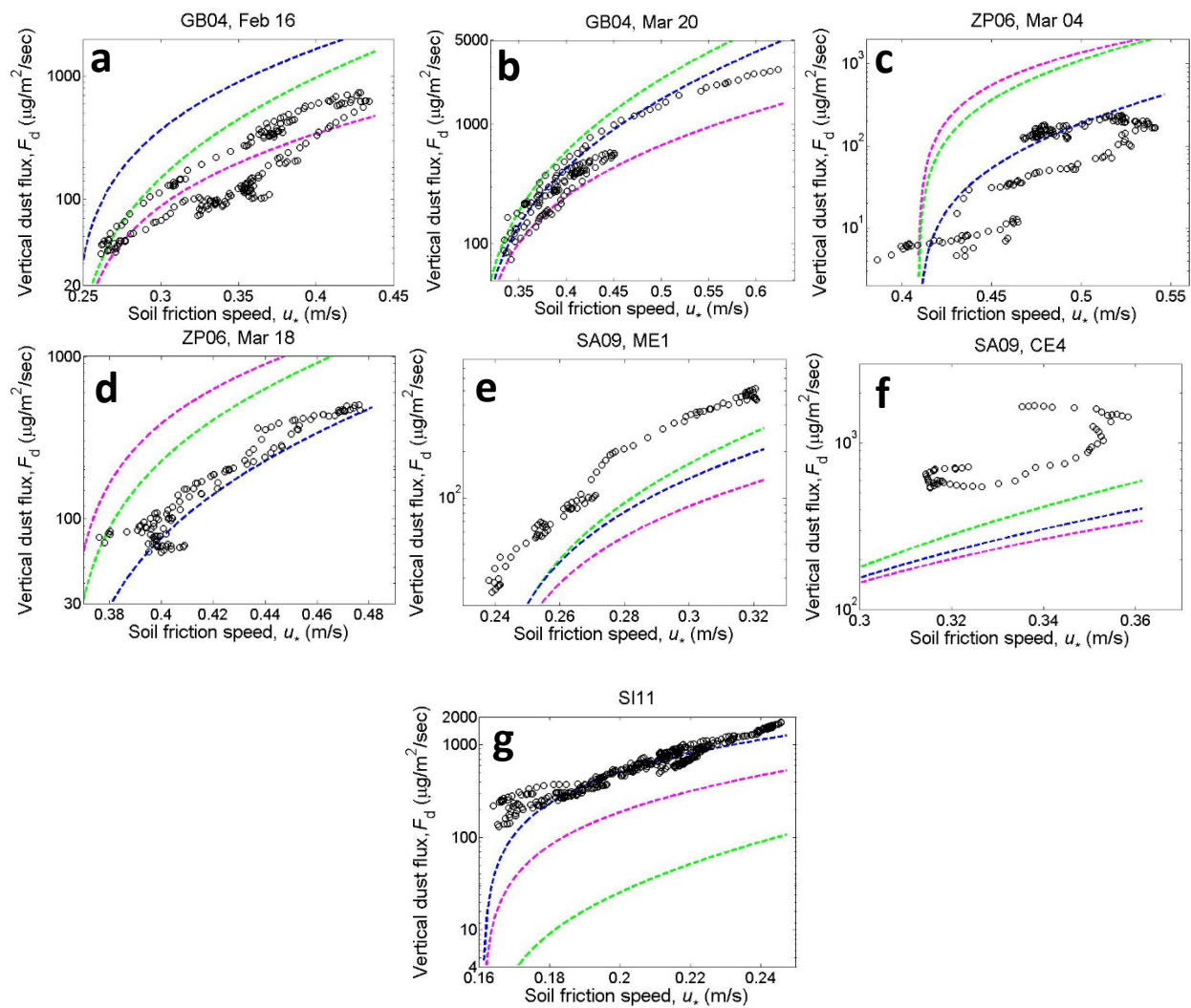


Figure S3. Same as Fig. S2, except that the proportionality constants in the three parameterizations was not tuned. Only data sets that meet the horizontal homogeneity-criteria, and can thus be used in Fig. 5, are plotted.

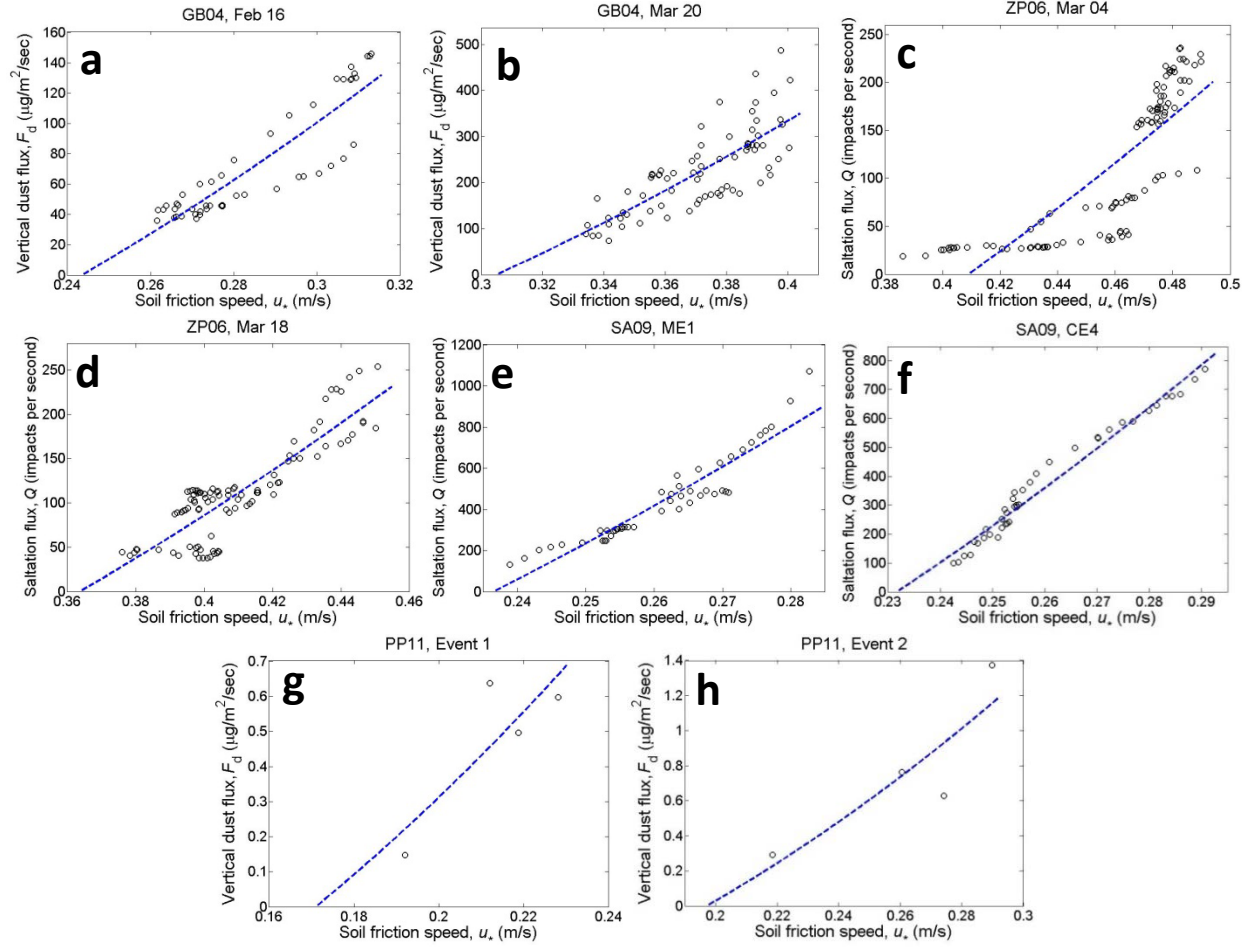


Figure S4. Estimation of the threshold friction velocity u_{*t} using the Taylor expansion method (Eqs. B.1, B.2) for each of the 8 data sets for which this method was possible. The estimation of u_{*t} for the other 3 data sets is discussed in the text.

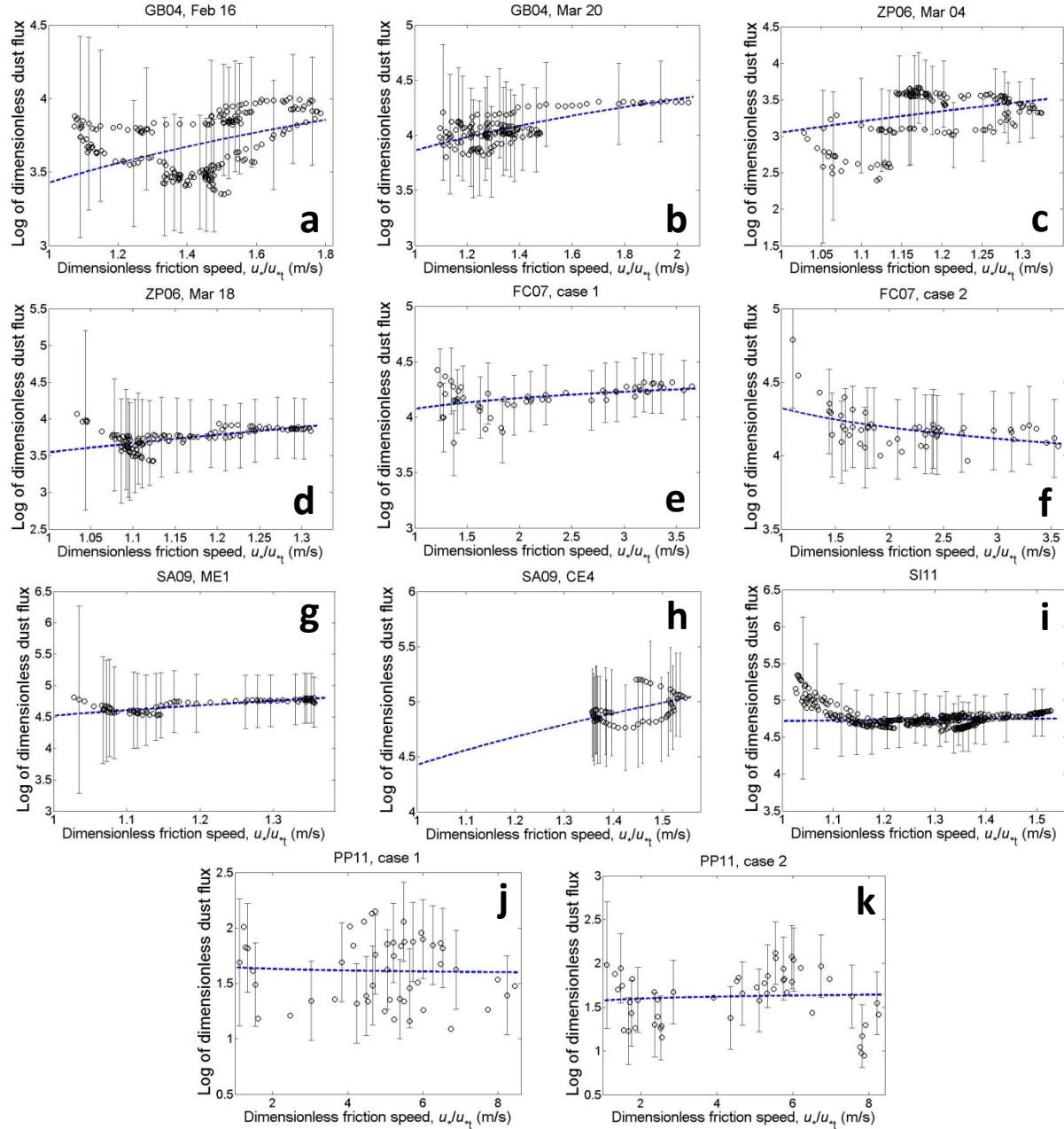


Figure S5. Estimation of the parameters α and C_d through fitting of the dimensionless dust flux (dashed blue line) as a function of dimensionless friction velocity to measurements (symbols) using Eq. (22) for each of the 11 data sets. Uncertainties on measurements were obtained as described in Appendix A, and plotted only for select data points to avoid clutter.

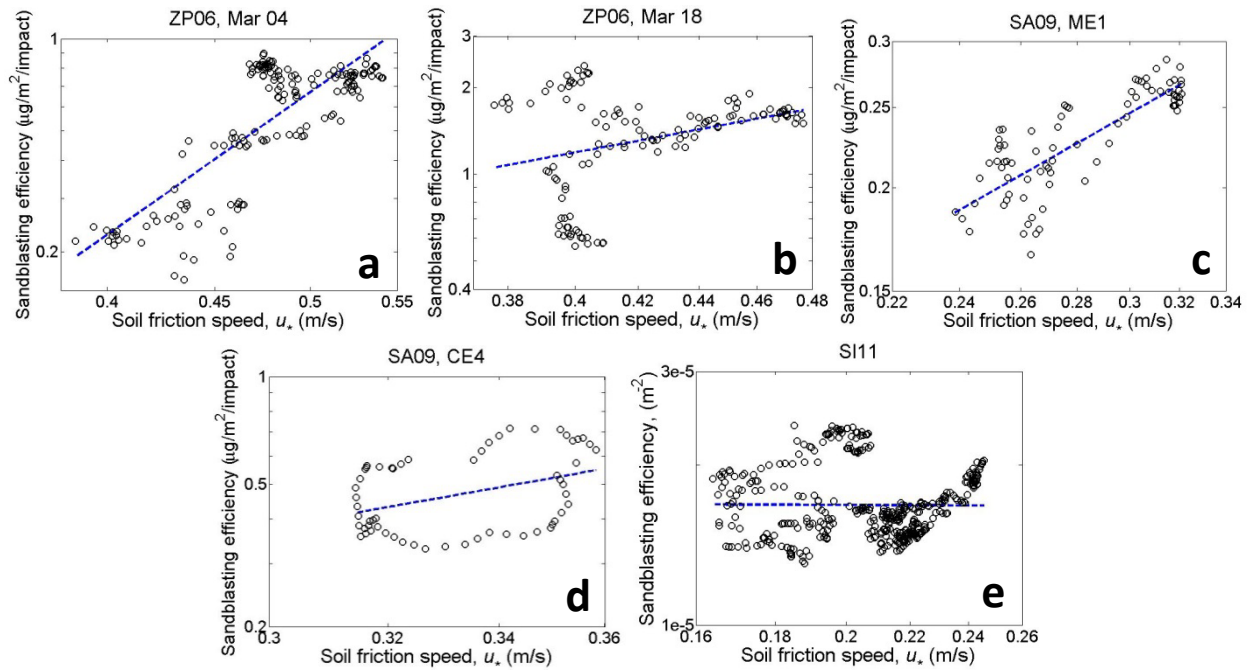


Figure S6. Estimation of the fragmentation exponent α by fitting the sandblasting efficiency (dashed blue line) as a function of the friction velocity using Eq. (25) for each of the 5 data sets for which use of this method was feasible.